# Stark Profiles of Hydrogen Spectral Lines under the Low-Frequency Laser Field in Turbulent Plasmas

E. Dalimier<sup>1</sup>, P. Angelo<sup>1</sup>, and E. Oks<sup>2</sup>\*

<sup>1</sup>LULI - Sorbonne Université ; CNRS, Ecole Polytechnique, CEA : Université Paris-Saclay – F-75252 Paris Cedex 05, France

<sup>2</sup>Physics Department, 380 Duncan Drive, Auburn University, Auburn, AL 36849, USA

#### Abstract

Stark broadening of spectral lines is an important tool for diagnostics of laboratory and astrophysical plasmas. In particular, in studies of laser-plasma interactions, advanced methods of the diagnostics, based on the Stark broadening of spectral lines, revealed the rich physics of processes at the surface of the critical density including the development of the electrostatic plasma turbulence. At the relatively high amplitudes  $E_0$  of the laser field at the frequency  $\omega$ , at the surface of the critical density (or the relativistic critical density), there was diagnosed spectroscopically the combination of a Low-frequency Electrostatic Plasma Turbulence (LEPT), such as e.g., ion acoustic waves, and the "high-frequency" quasimonochromatic electric field of Langmuir waves. In the present paper we consider the situation where the amplitude  $F_0$  and/or the frequency  $\omega$  of the laser field is smaller than in the above experiments, so that the radiating hydrogen atom (the radiator) does not "feel" the dynamical nature of the laser field: the radiator perceives not only the LEPT as quasistatic (which is practically always the case), but also the laser field as quasistatic. We focused on the situation where the plasma ion microfield is not quasistatic, but rather produces the dynamical Stark broadening, just as the plasma electrons. In this situation the quasistatic fields in the plasma are either the linearly-polarized laser field F and the *colinear* field  $\mathbf{E}_1$  of the LEPT, or the circularly-polarized laser field  $\mathbf{F}$  and the *coplanar* field  $\mathbf{E}_1$  of the LEPT We calculated analytically the distribution of the total quasistatic field  $\mathbf{E} = \mathbf{F} +$  $\mathbf{E}_1$  and provided the illustration. Then we calculated analytically the Stark profiles of the Ly-beta line (with the allowance for the dynamic Stark broadening by the plasma microfield) for various combinations of the dynamical Stark halfwidth  $\gamma$  and the ratio of the laser field amplitude  $F_0$  to the root-mean-square LEPT field E<sub>0</sub>. We studied the evolution of the Ly-beta profiles as the ratio  $f = F_0/E_0$  changes at fixed  $\gamma$ , and as  $\gamma$  changes at fixed f. We believe that our results can be important for the spectroscopic studies of the laser-plasma interactions.

Key words: laser-plasma interactions; lineshape-based spectroscopic diagnostics; low-frequency electrostatic plasma turbulence; distributions of the total quasistatic electric field

\*Corresponding author email: <a href="mailto:oksevgu@auburn.edu">oksevgu@auburn.edu</a>

#### 1. Introduction

Stark broadening of spectral lines is an important tool for diagnostics of laboratory and astrophysical plasmas – see, e.g., books [1-5] (listed in the chronological order) and references therein. In particular, in studies of laser-plasma interactions, advanced methods of the diagnostics, based on the Stark broadening of spectral lines, revealed the rich physics of

processes at the surface of the critical density including the development of the electrostatic plasma turbulence. These has been done in many experiments employing laser frequencies spanning from the microwave range (as, e.g., in experiments [6-11] covered also in book [12]) to the near infrared range- as, e.g., in experiments [13, 14] (covered also in review [15]) studying relativistic laser-plasma interactions). Here we use the world "laser" in a broad sense – referring to a beam of a quasimonochromatic electromagnetic radiation regardless of its frequency.

At the relatively high amplitudes  $F_0$  of the laser field at the frequency  $\omega$ , at the surface of the critical density (or the relativistic critical density as in experiments [13, 14]), there was diagnosed spectroscopically the combination of a Low-frequency Electrostatic Plasma Turbulence (LEPT), such as e.g., ion acoustic waves at the frequencies

$$\omega \le \omega_{\rm pi} = (4\pi e^2 N_i Z_i^2 / m_i)^{1/2},$$
 (1)

 $(\omega_{pi})$  being the plasma ion frequency), and the "high-frequency" quasimonochromatic electric field of Langmuir waves – the waves at the plasma electron frequency

$$\omega_{\rm pe} = (4\pi e^2 N_{\rm e}/m_{\rm e})^{1/2}.$$
 (2)

In Eqs. (1) and (2),  $N_i$  and  $N_e = Z_i N_i$  are the ion and electron densities, respectfully;  $Z_i$  and  $m_i$  are the charge and mass of plasma ions, respectively; e and  $m_e$  are the electron charge and mass, respectively. Under the joint action of the Langmuir waves and the LEPT, narrow "bump-dip-bump" structures (called for brevity L-dips) show up at specific locations of the experimental profiles of hydrogenic spectral lines. It should be emphasized that from the theoretical viewpoint, L-dips, manifest *multifrequency nonlinear dynamic resonances* (see, e.g., papers [13, 15] and books [2, 7]). The theoretical predictions of the L-dips were validated in a large numerous experiments by various experimental groups employing different plasma sources - plus in astrophysical observations. In these experiments and observations, covering about ten orders of magnitude with respect to the electron density, the L-dips were dependably identified and utilized for plasma diagnostics – see, e.g., review [15] and references therein.

In the present paper we consider the situation where the amplitude  $F_0$  and/or the frequency  $\omega$  of the laser field is smaller than in the above experiments, so that the radiating hydrogen atom does not "feel" the dynamical nature of the laser field. In other words, the radiating hydrogen atom perceived not only the LEPT as quasistatic (which is practically always the case because of the low-frequency of this electrostatic turbulence, more details being presented in Appendix A), but also the laser field as quasistatic (so that L-dips are not possible). The corresponding validity condition, derived in section 3.1.1 of book [12] is the following:

$$CF_0\omega^2 \ll 1/\tau_{life}^3, \tag{3}$$

where  $\tau_{life}$  is the lifetime of the excited state (i.e., of the upper energy level) of the radiating hydrogen atom (hereafter, radiator), from which the spectral line originates. In Eq. (3), C is the following Stark constant averaged over the Stark components of the spectral line

$$C = 3n^2\hbar/(4m_ee),$$
 (4)

where n is the principal quantum number of the upper level.

Since the development of the LEPT (by which here and below we mean either the ion acoustic waves or Bernstein modes) occurs at the surface of the critical density where  $\omega = \omega_{pe}$ , then the condition (3) takes the form

$$CF_0\omega_{pe}^2 << 1/\tau_{life}^3.$$
 (5)

Typically, the inverse lifetime of the excited state is

$$1/\tau_{life} = \gamma_i + \gamma_e + \gamma_r, \tag{6}$$

where  $\gamma_i$  and  $\gamma_e$  are the Stark widths due to the dynamic plasma ions and plasma electrons, respectively;  $\gamma_r$  is the radiative width.

We focus on the situation where the plasma ion microfield is not quasistatic (from the point of view of the radiating hydrogen atom), but rather produces the dynamical Stark broadening, just as the plasma electrons. The corresponding validity condition is (allowing for  $N_i = N_e$ ):

$$(4\pi\rho_{wi}^{3}/3)N_{i}<1. \tag{7}$$

Here

$$\rho_{\rm wi} \approx n^2 \hbar / (m_{\rm e} v_{\rm Ti}),$$
(8)

is the ion Weisskopf radius;  $v_{Ti}$  is the mean thermal velocity of plasma ions of the temperature T. Physically, the condition (7) means that the number of perturbing ions in the sphere of the ion Weisskopf radius is smaller than unity – see, e.g., review [16]. After allowing for  $N_i = N_e$ , the condition (7) becomes:

$$(4\pi\rho_{wi}^{3}/3)N_{e}<1. \tag{9}$$

Below we analyze the following two situations. One situation is where the quasistatic fields in the plasma are only the linearly-polarized laser field  $\mathbf{F}$  and the *colinear* field  $\mathbf{E}_1$  of the LEPT (such as, e.g., ion acoustic waves). Another situation is where the quasistatic fields in the plasma are only the circularly-polarized laser field  $\mathbf{F}$  and the *coplanar* circularly-polarized field  $\mathbf{E}_1$  of the LEPT (such as, e.g., Bernstein modes, ion cyclotron waves, or lower hybrid oscillations). Details on the validity conditions and specific examples of the plasma and field parameters are given in Appendix A.

In the present paper, for both of the above situations, first we calculate analytically the distribution of the total quasistatic field  $\mathbf{E} = \mathbf{F} + \mathbf{E}_1$  and illustrate it pictorially. Then we calculate analytically the Stark profiles of the Ly-beta line (with the allowance for the dynamic Stark broadening by the plasma microfield) for various combinations of dynamical Stark width and the ratio of the laser field amplitude  $F_0$  to the root-mean-square LEPT field  $E_0$ .

# 2. Analytical results and illustrations for colinear fields

The distributions of various kinds of the LEPT were calculated analytically in papers [17, 18]. In particular, for the linearly-polarized LEPT the distribution is

$$W_{\text{LEPT}}(E_1) = \{1/[(2\pi)^{1/2}E_0]\} \exp[-E_1^2/(2E_0^2)], \quad -\infty < E_1 < \infty.$$
 (10)

The distribution of the quasistatic laser field F is (see, e.g., section 3.1.1 of book [12]):

$$W_{las}(F) = 1/[\pi(F_0^2 - F^2)^{1/2}], \quad -F_0 \le F \le F_0.$$
(11)

The distribution of the total field E is

$$W(E) = \int_{-\infty}^{\infty} dE_1 \int_{-F_0}^{F_0} dF \ W_{LEPT}(E_1) \ W_{las}(F) \ \delta(E - E_1 - F), \tag{12}$$

where  $\delta(...)$  is the Dirac delta-function. By using the properties of the  $\delta$ -function, we find

$$\begin{split} W(E) = & \int\limits_{-F_0}^{F_0} \! dF \; W_{las}(F) \; \{1/[(2\pi)^{1/2}E_0]\} exp[-(E-F)^2/(2E_0^2)] = \\ \{1/[(2^{1/2}\pi^{3/2}E_0]] \int\limits_{-F_0}^{F_0} \! dF \; (F_0^2 - F^2)^{-1/2} exp[-(E-F)^2/(2E_0^2)]. \end{split} \label{eq:WE} \end{split}$$

We introduce the following dimensionless quantities:

$$\varepsilon = E/E_0, f = F_0/E_0, u = F/E_0.$$
 (14)

Then in terms of the scaled total field  $\varepsilon$ , the distribution from Eq. (13) transforms into

$$W(\varepsilon, f) = \left[1/(2^{1/2}\pi^{3/2})\right] \int_{-f}^{f} du (f^2 - u^2)^{-1/2} \exp[-(\varepsilon - u)^2/2].$$
 (15)

Figure 1 shows the three-dimensional plot of  $W(\varepsilon, f)$ .

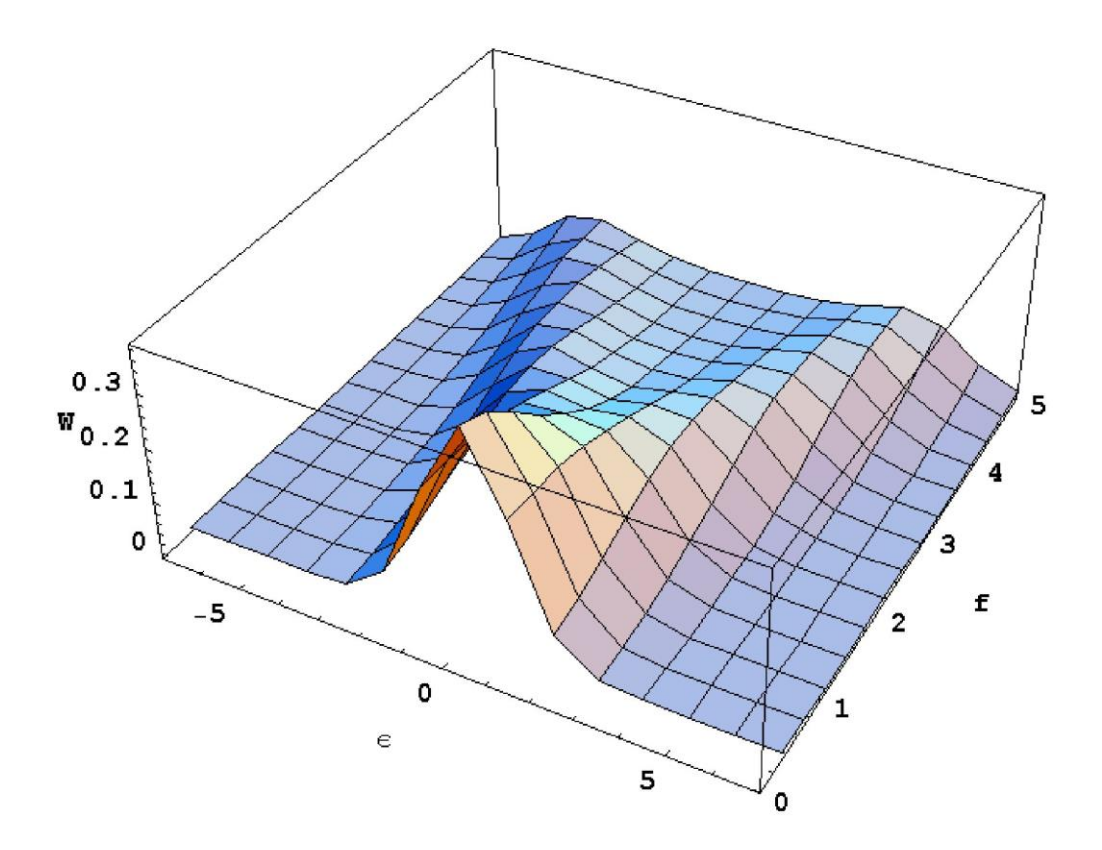


Fig. 1. Three-dimensional plot of the distribution  $W(\epsilon, f)$ , where  $\epsilon = E/E_0$  is the scaled total quasistatic field and  $f = F_0/E_0$  is the ratio of the amplitude of the laser field to the root-mean-square value of the LEPT field.

Based on this distribution, we calculated analytically Stark profiles of the hydrogen Ly-beta line for several combinations of the input parameters. For the Stark profiles of the Ly-beta line at the fixed value of the total quasistatic field we used the corresponding analytical results from Strekalov-Burshtein paper [19]. According to that paper, the profile consists of the combination of several subprofiles of the form

$$S_{j}(\Delta\omega) = (1/\pi)\Gamma_{j}/[\Gamma_{j}^{2} + (\Delta\omega - a_{j}E)^{2}]. \tag{16}$$

In Eq. (16),  $\Gamma_j$  and  $a_j$  are the dynamical Stark width and the Stark constant of the subcomponent j, respectively.

We denote

$$D = \Delta \omega/(kE_0), \hspace{1cm} \gamma_j = \Gamma_j/(kE_0), \hspace{1cm} k = 3\hbar/(2m_e e). \hspace{1cm} (17)$$

Then in these scaled notations, the Stark profiles of the Ly-beta line become

$$S(D, f) = (1/\pi) \int_{0}^{\infty} d\varepsilon W(\varepsilon, f) \sum_{i} I_{j} \gamma_{j} / [\gamma_{j}^{2} + (D - a_{j}\varepsilon/k)^{2}], \qquad (18)$$

where  $I_j$  is the statistical weight of the subcomponent j.

The next several figures demonstrate the calculated scaled Stark profile  $S(f, \gamma, D)$  of the Lybeta line for various combinations of the ratio  $f = F_0/E_0$  and of the largest (among the subcomponents) scaled dynamical Stark width  $\gamma$ . In particular, Fig. 2 shows S(10, 1, D).

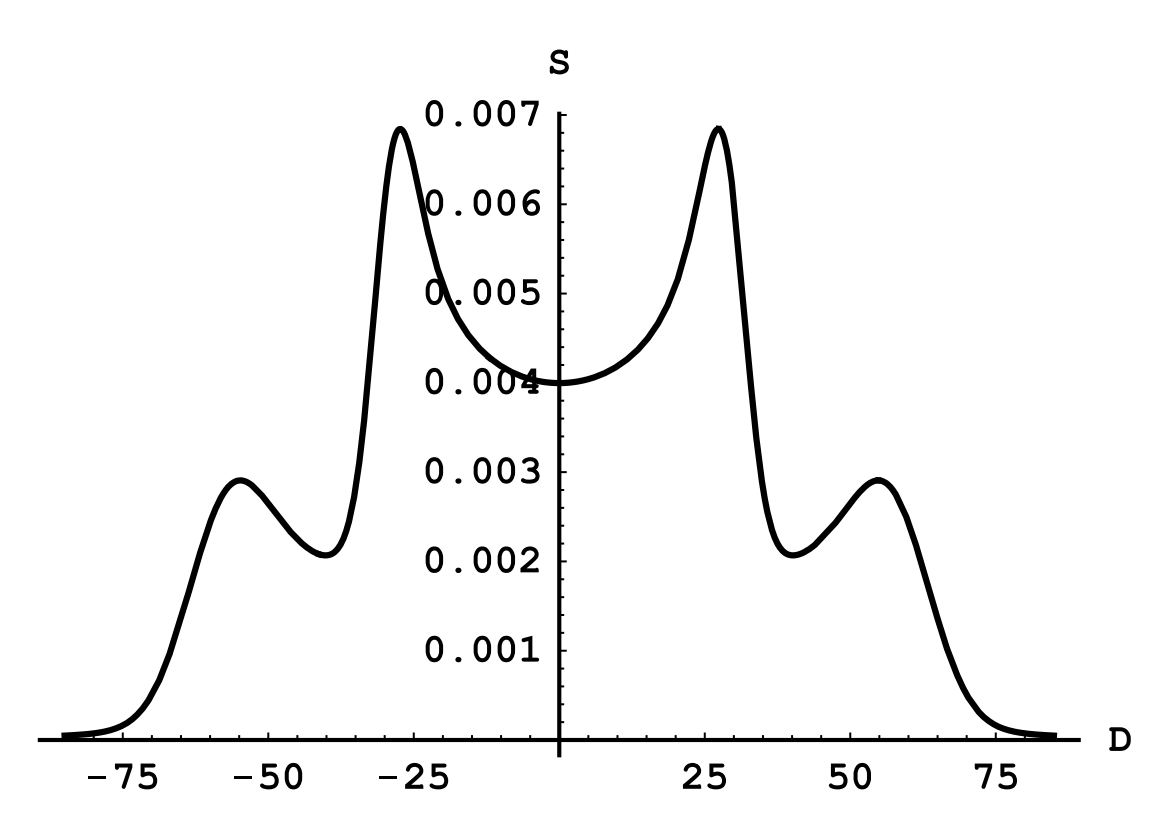


Fig. 2. Calculated scaled Stark profile  $S(f, \gamma, D)$  of the Ly-beta line for  $f = F_0/E_0 = 10$  and  $\gamma = 1$ , where  $\gamma$  is the largest (among the subcomponents) scaled dynamical Stark width.

Figure 3 presents S(5, 1, D).

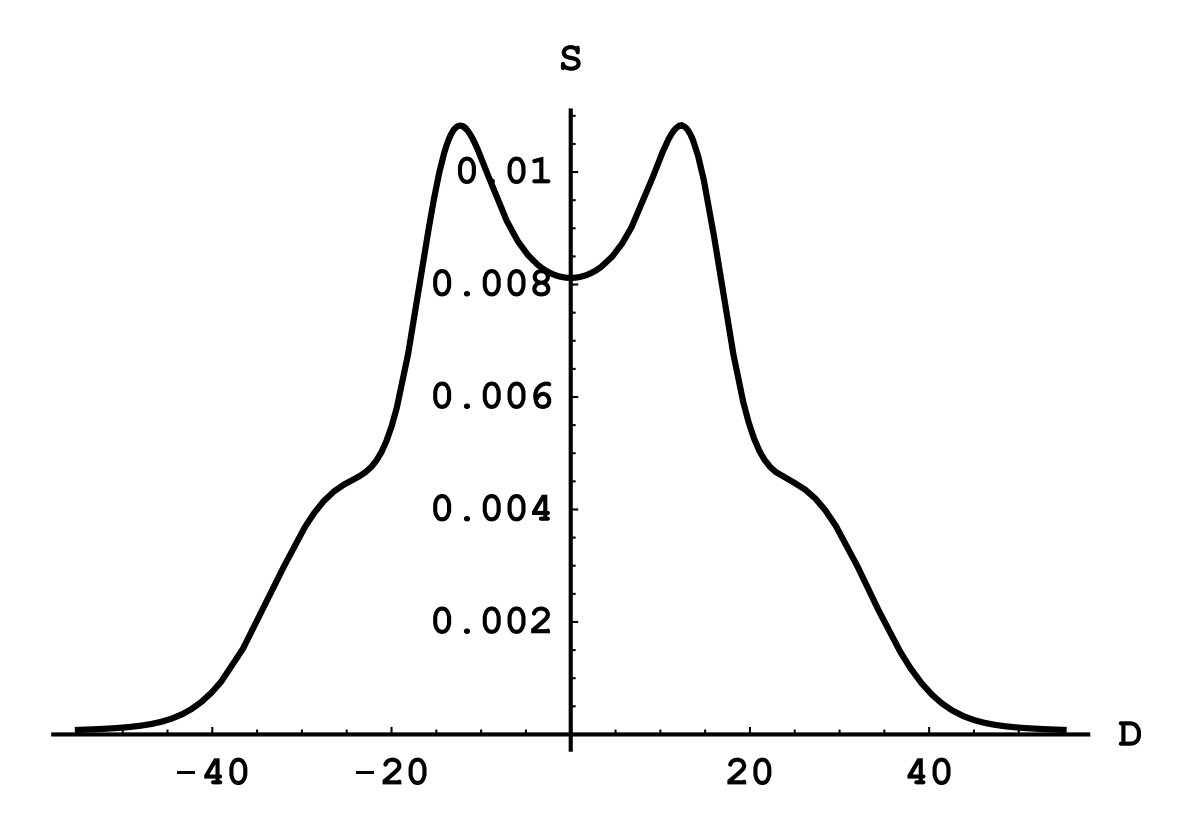


Fig. 3. The same as in Fig. 2, but for f = 5 and  $\gamma = 1$ .

Figure 4 displays S(1, 1, D).

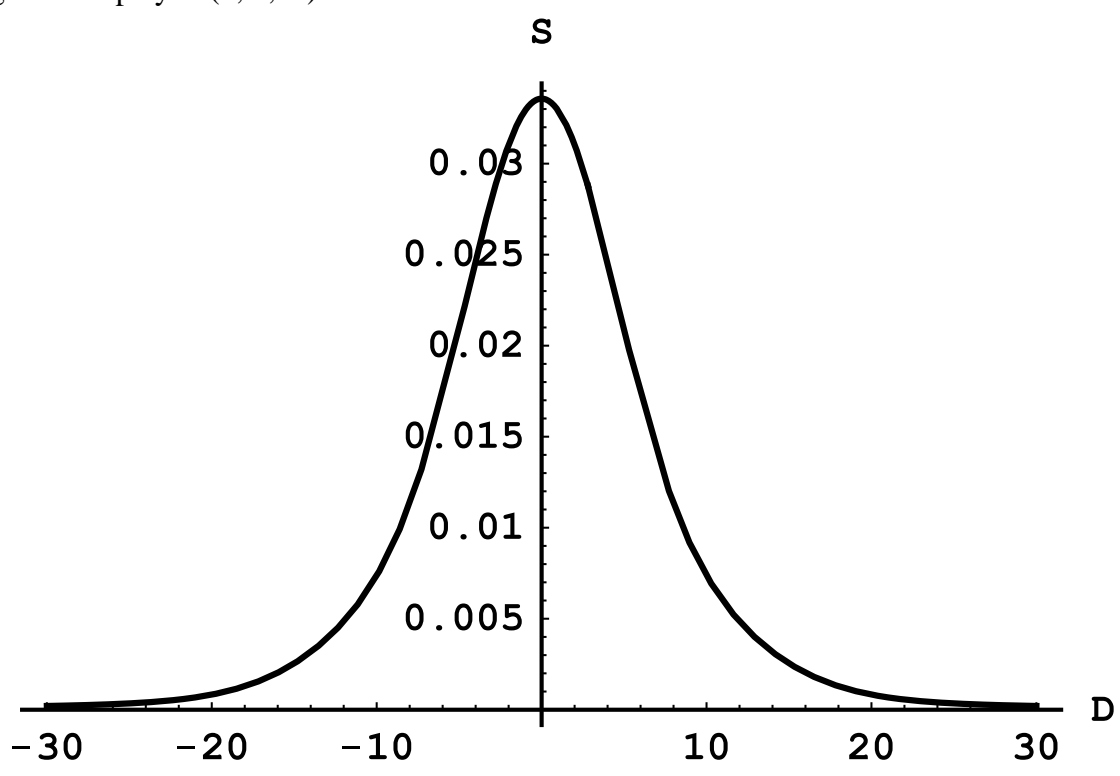


Fig. 4. The same as in Fig. 2, but for f=1 and  $\gamma=1$ .

From Figs. 2-4 it is seen that as the ratio  $f = F_0/E_0$  decreases at fixed  $\gamma$ , first the furthest lateral maxima become just shoulders. As the ratio f further decreases, all lateral maxima disappear. Figure 5 demonstrates S(5, 3, D).

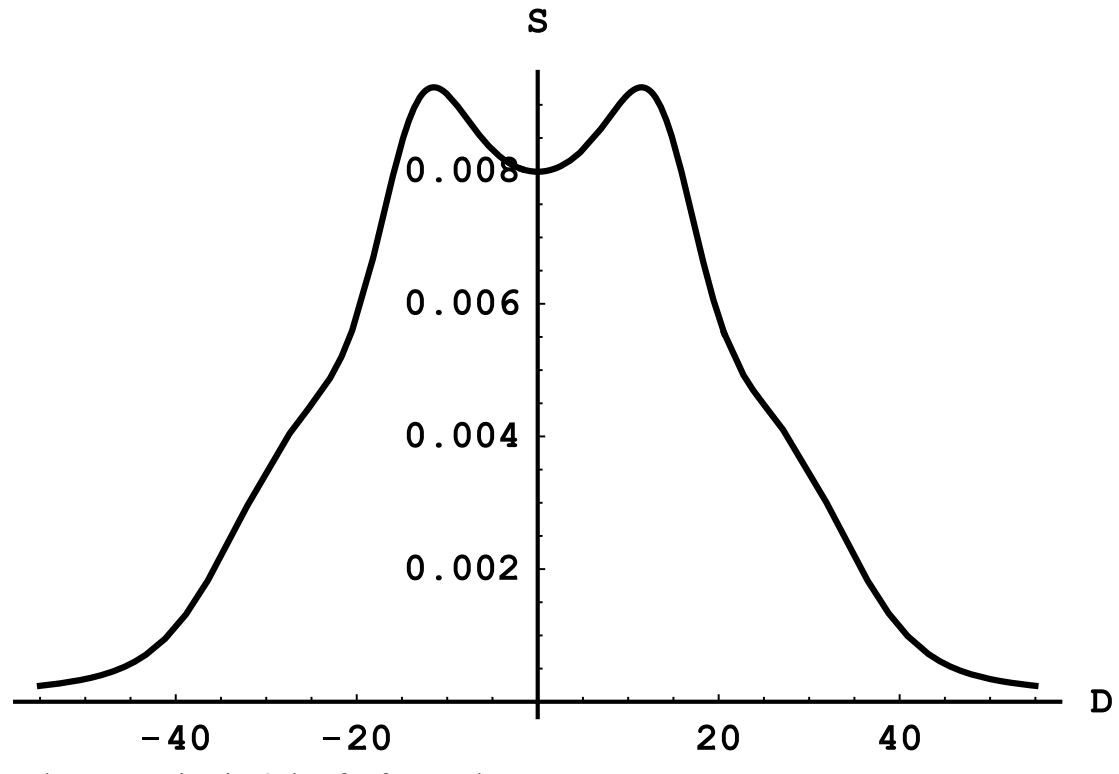


Fig. 5. The same as in Fig. 2, but for f = 5 and  $\gamma = 3$ .

Figure 6 displays the same as in Fig. 2, but for f = 5 and  $\gamma = 20$  (solid line). The corresponding Lorentzian of the half width at half maximum equal to  $\gamma = 20$  is shown by the dashed line.

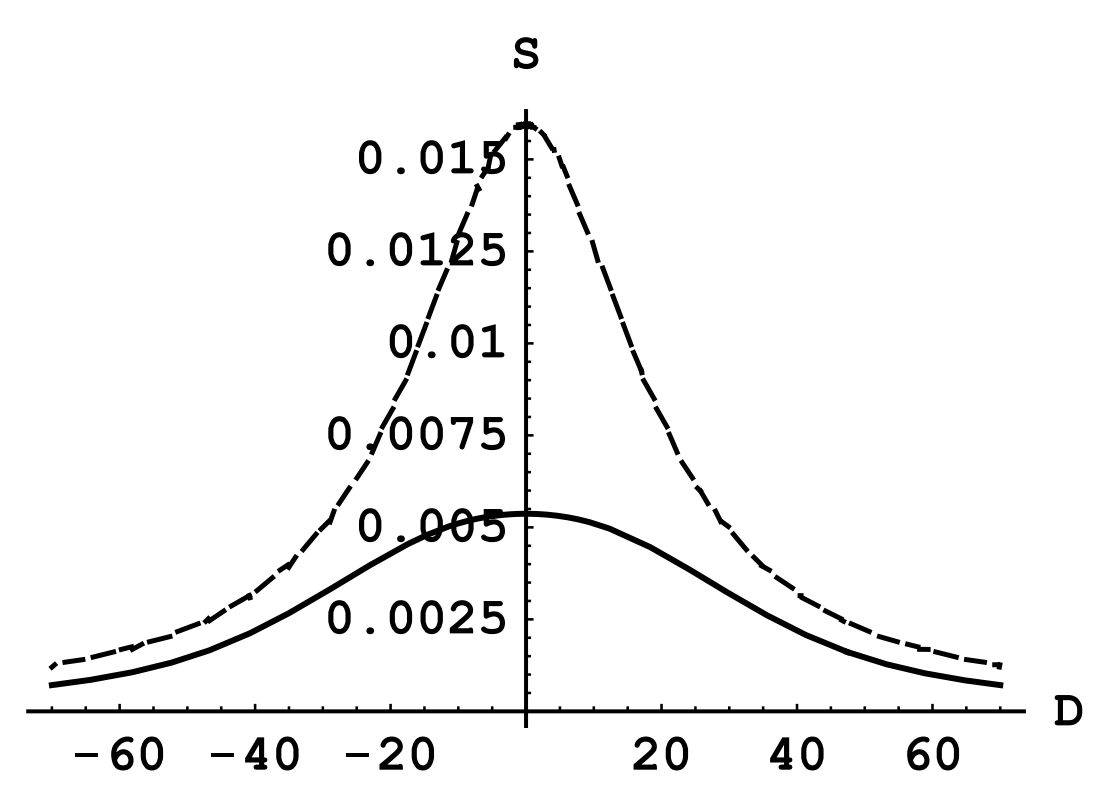


Fig. 6. The same as in Fig. 2, but for f = 5 and  $\gamma = 20$  (solid line). The corresponding Lorentzian of the half width at half maximum equal to  $\gamma = 20$  is shown by the dashed line.

From Figs. 5 and 6 it is seen that as the dynamical Stark width  $\gamma$  increases at the fixed ratio  $f = F_0/E_0$ , first the furthest lateral maxima become just shoulders. As  $\gamma$  further increases, all lateral maxima disappear. Nevertheless, the Stark profile remains significantly broader than the corresponding Lorentzian of the half width at half maximum equal to  $\gamma$ , as shown in Fig. 6.

# 3. Analytical results and illustrations for coplanar fields

The quasistatic circularly polarized laser field has the amplitude F. The LEPT distribution is the following two-dimensional distribution in the plane of the two fields:

$$W_2(E_1) dE_1 = (2E_1/E_{10})\exp[-E_1^2/E_{10}^2] dE_1.$$
 (19)

This situation is typical for the Bernstein modes and the lower hybrid waves. Obviously in this case the total electric field  $\mathbf{E} = \mathbf{E}_2 + \mathbf{F}$  is confined in the plane of the two fields. Its distribution has the form:

W(E) dE = 
$$dE (1/\pi) \int_{0}^{\infty} dE_1 W_2(E_1) \int_{0}^{\pi} d\psi \, \delta[E - (E_1^2 + F^2 + 2E_1F\cos\psi)^{1/2}].$$
 (20)

After using the  $\delta$ -function to perform the integration over the angle  $\psi$  (which is the angle between vectors  $\mathbf{E}_1$  and  $\mathbf{F}$ ), the result reduces to the following:

$$\begin{aligned} W(E) \; dE &= \\ &\stackrel{Emax}{dE} \; (21) \\ dE \; (E/\pi) \int\limits_{Emin}^{\int} dE_1 \; W_2(E_1) \; \Theta(E-F)/\{[(\; E_1 + F)^2 - E^2][\; E^2 - (E_1 - F)^2]\}^{1/2}. \end{aligned}$$

In Eq. (3),  $\Theta(E-F)$  is the Heaviside step function; the lower and upper limits of the integration over  $E_L$  are

$$E_{min} = E - F$$
,  $E_{max} = E + F$ . (22)

We proceed to the scaled notations:

$$\varepsilon = E/E_{10}, \qquad f = F/E_{10}, \qquad u = E_2/E_{10}.$$
 (23)

In these notations, the scaled distribution of the total field takes the form:

$$w_{scaled}(f,\,\epsilon) = (2/\pi) \int_{\epsilon-f}^{\epsilon+f} du \ u \ exp[-u^2] \ \Theta(\epsilon-f)/\{[(\ u+f)^2-\epsilon^2][\ \epsilon^2-(u-f)^2]\}^{1/2}. \eqno(24)$$

As example, Figure 7 presents the plots of the scaled distribution  $w_{scaled}(f, \epsilon)$  for f = 0.5 and f = 2, respectively.

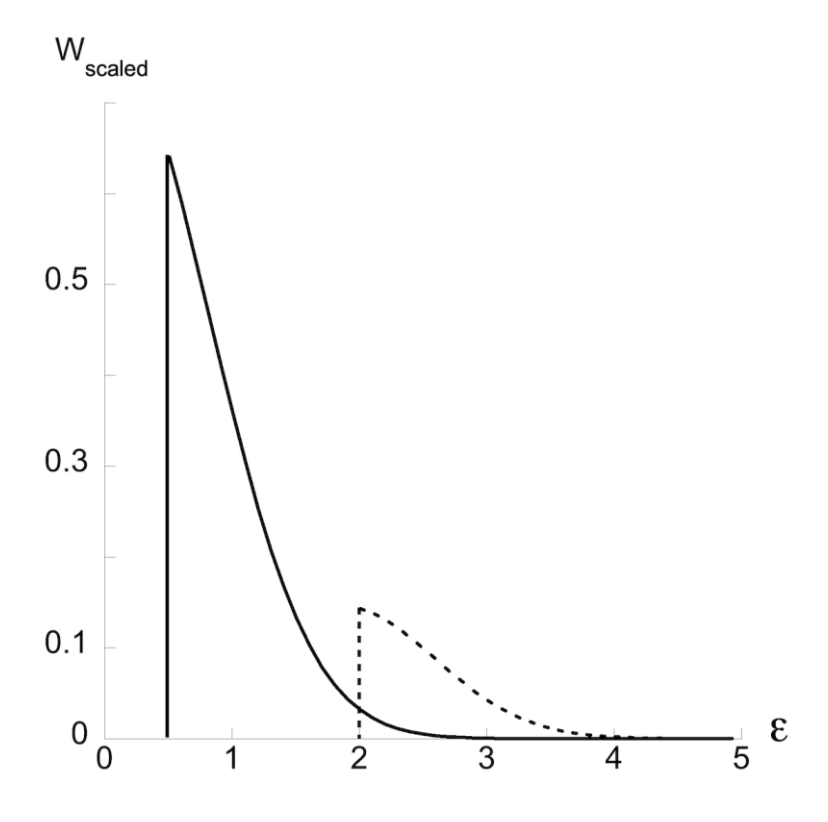


Fig. 7. The scaled distribution  $w_{\text{scaled}}(f, \varepsilon)$  for f = 0.5 (solid line) and f=2 (dashed line).

We note that the "truncation" of the distributions in Fig. 7 at some value of  $\epsilon$  is due to the presence of the Heaviside step function  $\Theta(\epsilon - f)$  in the integrand of Eq. (24).

Further we denote

$$D = \Delta\omega/(kE_0), \qquad \gamma_i = \Gamma_i/(kE_0), \qquad k = 3\hbar/(2m_e e). \tag{17}$$

Then in these scaled notations, the Stark profiles of the Ly-beta line become

$$S(D, f) = (1/\pi) \int_{0}^{\infty} d\varepsilon W(\varepsilon, f) \sum_{i} I_{j} \gamma_{j} / [\gamma_{j}^{2} + (D - a_{j}\varepsilon/k)^{2}], \qquad (18)$$

The next several figures demonstrate the scaled Stark profile  $S(f, \gamma, D)$  of the Ly-beta line in the observation perpendicular to the plane of the fields, calculated similarly to those in section 2. The figures present  $S(f, \gamma, D)$  for various combinations of the ratio  $f = F_0/E_0$  and of the largest (among the subcomponents) scaled dynamical Stark width  $\gamma$ .

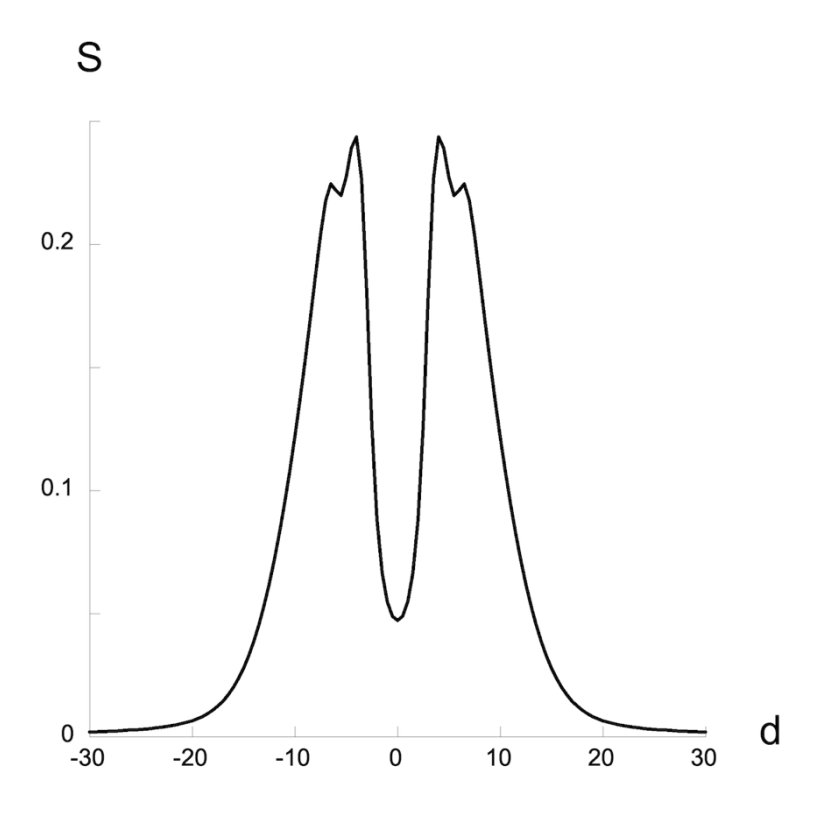


Fig. 8. Calculated scaled Stark profile  $S(f, \gamma, D)$  of the Ly-beta line for f = 1 and  $\gamma = 1$ .

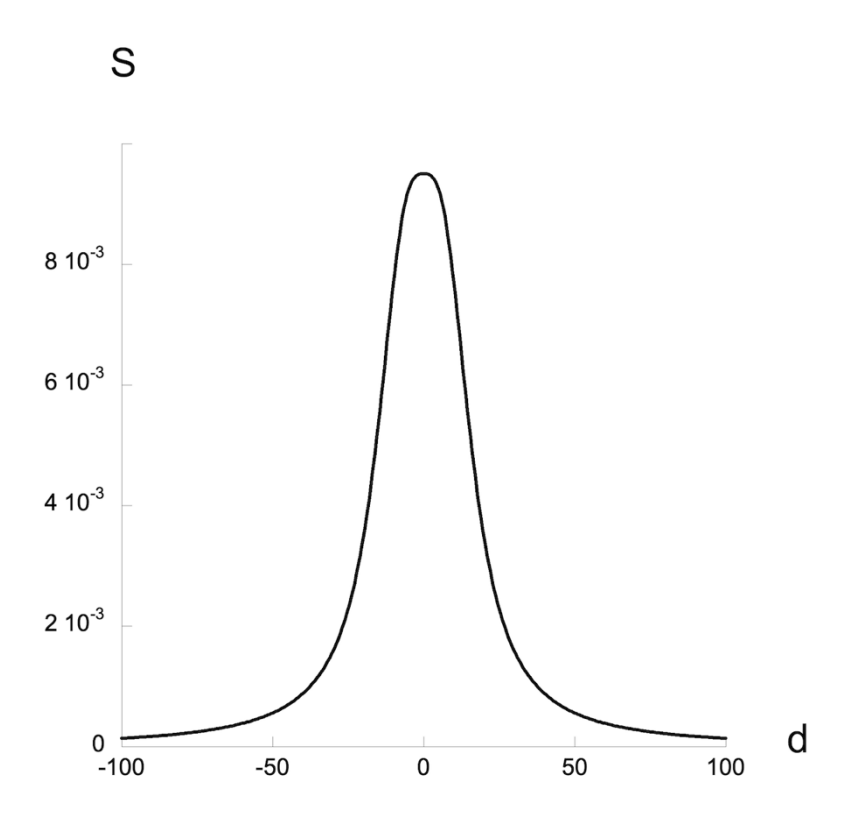


Fig. 9. Calculated scaled Stark profile  $S(f, \gamma, D)$  of the Ly-beta line for f=1 and  $\gamma=10$ .

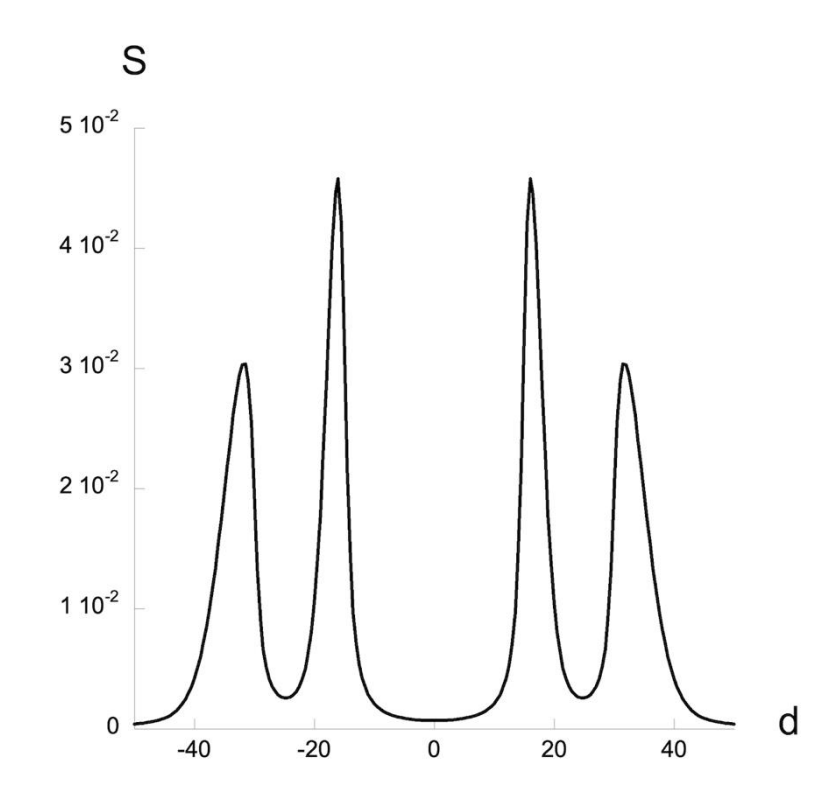


Fig. 10. Calculated scaled Stark profile  $S(f,\gamma,D)$  of the Ly-beta line for f=5 and  $\gamma=1$ .

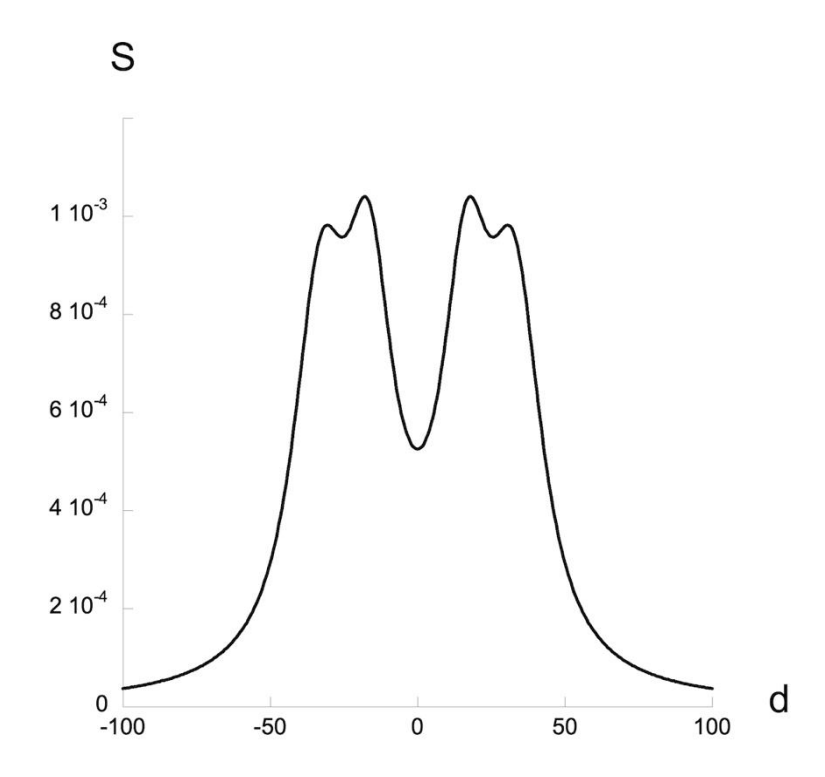


Fig. 11. Calculated scaled Stark profile  $S(f, \gamma, D)$  of the Ly-beta line for f = 5 and  $\gamma = 10$ .

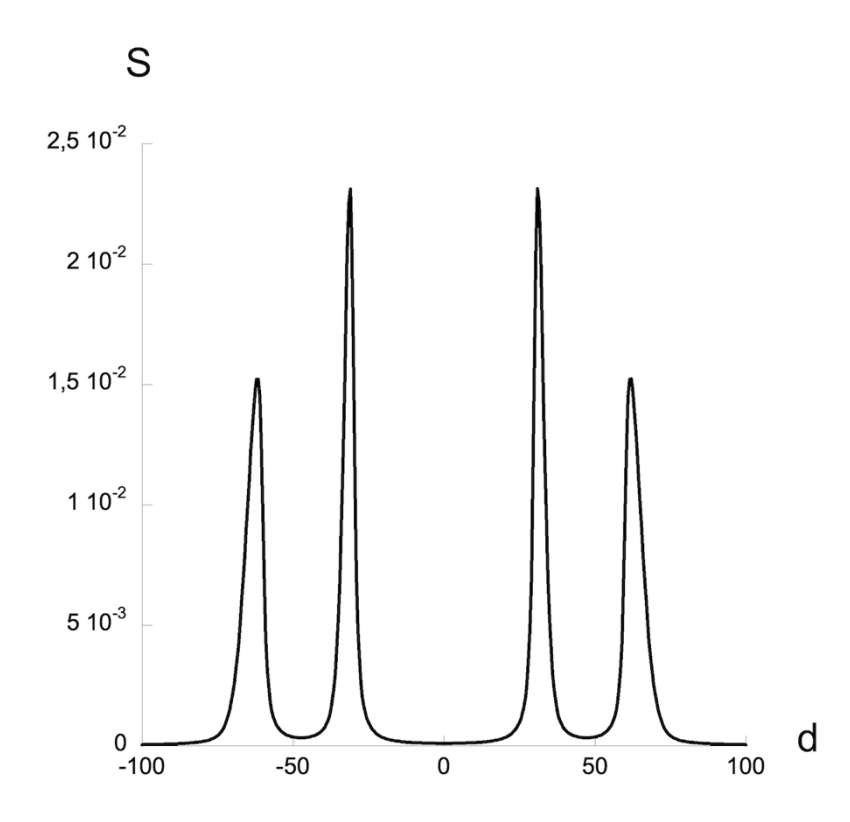


Fig. 12. Calculated scaled Stark profile  $S(f,\gamma,D)$  of the Ly-beta line for f=10 and  $\gamma=1$ .

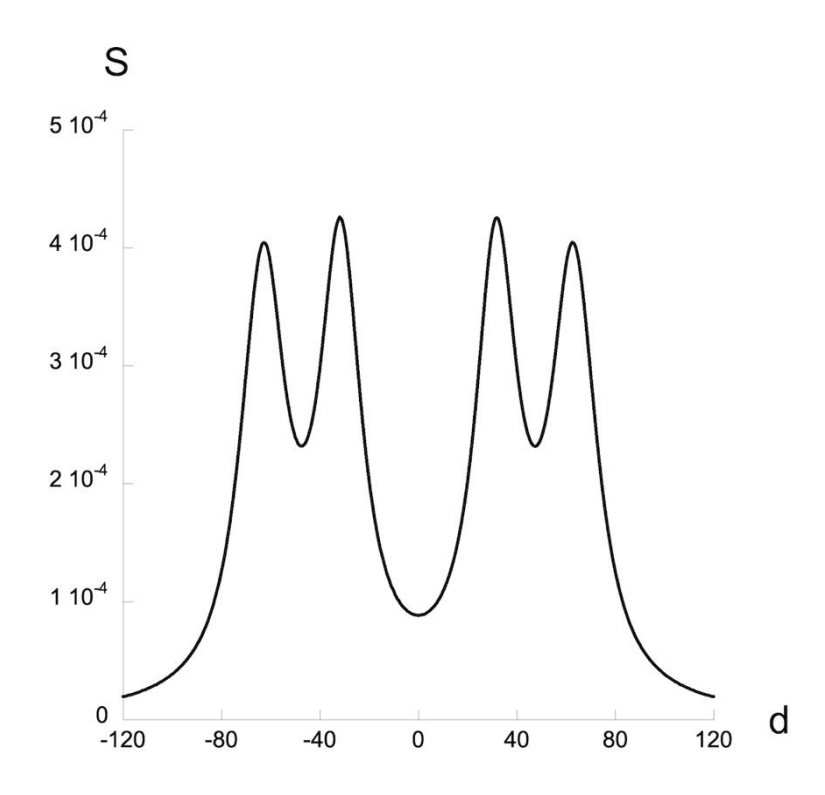


Fig. 13. Calculated scaled Stark profile  $S(f, \gamma, D)$  of the Ly-beta line for f = 10 and  $\gamma = 10$ .

From Figs. 8-13, one can see the following. At  $f << \gamma$ , the Stark profile is structureless (see Fig. 9). At  $f \sim \gamma$ , where  $f \le 5$ , the Stark profiles exhibit two maxima: one in the blue part (d > 0) and the other in the red part (d < 0) – see, Figs. 8 and 11. At  $f = \gamma = 10$ , the Stark profiles exhibit four maxima: one in the blue part and the other in the red part – see Fig. 13. At  $f >> \gamma$ , these four maxima become much more pronounced and isolated from each other – see Figs. 10 and 12.

### 4. Conclusions

In many experimental studies of laser-plasma interactions, at the surface of the critical density (or the relativistic critical density), the development of the LEPT, such as e.g., ion acoustic waves, has been diagnosed spectroscopically (in addition to the development of the Langmuir waves manifested as localized L-dips in the spectral line profiles). From the point of view of the radiating hydrogenic atom/ion, the LEPT was quasistatic.

In the present paper we analyzed the situation where the amplitude and/or the frequency of the laser field is smaller than in the above experiments, so that the radiating hydrogen atom does not sense the dynamic nature of the laser field. So, the radiating hydrogen atom perceived as quasistatic both the LEPT and the laser field (thus excluding the possibility of the L-dips).

We focused on the situation where the plasma ion microfield is not quasistatic, but rather produces the dynamical Stark broadening, just as the plasma electrons. In this situation the quasistatic fields in the plasma are either the linearly-polarized laser field  $\mathbf{F}$  and the *colinear* field  $\mathbf{E}_1$  of the LEPT (the latter being colinear with  $\mathbf{F}$  because the ion acoustic wave develops in the direction of  $\mathbf{F}$ ), or the circularly-polarized laser field  $\mathbf{F}$  and the *coplanar* field  $\mathbf{E}_1$  of the LEPT (such as, e.g., Bernstein modes, ion cyclotron waves, or lower hybrid oscillations).

We calculated analytically the distribution of the total quasistatic field  $\mathbf{E} = \mathbf{F} + \mathbf{E}_1$  and provided the illustration. Then we calculated analytically the Stark profiles of the Ly-beta line (with the allowance for the dynamic Stark broadening by the plasma microfield) for various combinations of the dynamical Stark halfwidth  $\gamma$  and the ratio of the laser field amplitude  $F_0$  to the root-mean-square LEPT field  $E_0$ .

For the case of the colinear fields, we demonstrated that as the ratio  $f = F_0/E_0$  diminishes at fixed  $\gamma$ , first the furthest lateral maxima of the Ly-beta profile become just shoulders, and that as the ratio f further decreases, all lateral maxima disappear. We also showed that as the dynamical Stark width  $\gamma$  increases at the fixed ratio  $f = F_0/E_0$ , first the furthest lateral maxima of the Ly-beta profiles become just shoulders, and as  $\gamma$  further increases, all lateral maxima disappear.

For the case of the coplanar fields, we showed that for  $f << \gamma$ , the Stark profile is structureless; at  $f \sim \gamma$ , where  $f \le 5$ , the Stark profiles exhibit two maxima: one in the blue part and the other in the red part; at  $f = \gamma = 10$ , the Stark profiles exhibit four maxima: one in the blue part and the other in the red part; at  $f >> \gamma$ , these four maxima become much more pronounced and isolated from each other.

We believe that our results can be important for the spectroscopic studies of the laser-plasma interactions.

## Appendix A. Validity conditions

The condition (9), under which the plasma ions produce mostly the dynamical Stark broadening, can be rewritten in the form of the restriction on the principal quantum number n:

$$n \le n_{cr,d} = 724 \ [T(eV)]^{1/4} / [N_e(cm^{-3})]^{1/6}. \tag{A.1}$$

Under the condition (A.1), the ion dynamical Stark broadening controls the lifetime  $\tau_{life}$  of the upper state of the radiating hydrogen atom:

$$1/\tau_{life} \sim \Gamma_i \sim [\pi n^4 \hbar^2 N_e/(m_e^2 v_{Ti})] [ln(\rho_{max}/\rho_{min}) + 1/2], \tag{A.2}$$

where  $v_{Ti}$  is the mean thermal velocity of plasma electrons;  $\rho_{max}$  and  $\rho_{min}$  are the upper and lower cutoff in the integration over the impact parameter  $\rho$  (see, e.g., review [16]); the term 1/2 in the utmost right brackets in Eq. (A.2) is the contribution of the so-called strong collisions. Typically,  $\rho_{max}$  is chosen as the Debye radius  $\rho_{De}$ 

$$\rho_{max}(cm) = \rho_{De}(cm) \approx 743 \ [T(eV)/N_e(cm^{-3})]^{1/2}, \eqno(A.3)$$

while  $\rho_{min}$  is chosen as the ion Weisskopf radius  $\rho_{wi}$  (see Eq. (8)):

$$\rho_{min}(cm) = \rho_{wi}(cm) \approx 1.18 \times 10^{-6} n^2 \{ \mu / [m_p T(eV)] \}^{1/2}. \tag{A.4}$$

In Eq. (A.4),  $\mu$  is the reduced mass of the radiator-perturber pair:

$$\mu \approx m_p m_i / (m_p + m_i), \tag{A.5}$$

where  $m_p$  is the proton mass.

In this situation, the condition (5) becomes

$$CE_0\omega^2 << \gamma_i^3, \tag{A.6}$$

what can be represented in the form  $F_0(V/cm) << F_{crit}(V/cm)$ , where

$$F_{crit}(V/cm) \approx 5.1 \times 10^{-34} n^{10} N_e^2 \{ ln[6.28 \times 10^8 n^{-2} T(eV)/Ne(cm^{-3})^{1/2}] + 1/2 \}^3 / [T(eV)]^{3/2}. \tag{A.7}$$

For completeness, we also present the condition, under which the LEPT (whose frequency is smaller or equal to  $\omega_{pi}$ ) is quasistatic because its field practically does not change during the lifetime of the excited state of the radiator:

$$\Gamma_i/\omega_{pi} \approx 3.25 \times 10^{-9} n^4 [Ne(cm^{-3})^{1/2}] \{ ln[6.28 \times 10^8 n^{-2} T(eV)/Ne(cm^{-3})^{1/2}] + 1/2 \} / [T(eV)^{1/2}] >> 1. \ (A.8)$$

As a numerical example, let us consider a plasma irradiated by a far-infrared "laser" of the frequency  $\nu=0.57$  THz: actually, the radiation of a gyrotron – now available at frequencies up to 1 THz [20]). The critical electron density, obtained from the equation  $\omega_{pe}=2\pi\nu$ , is  $N_{cr}\approx 4.0x10^{15}$  cm<sup>-3</sup>. Assuming the plasma temperature T=8 eV, we find from Eq. (A.1) that  $n_{cr,d}$  is slightly above 3. Therefore, for the hydrogen Ly-alpha and Ly-beta lines, as well as for the Balmer-alpha line, the lifetime of the excited state of the radiator is controlled by the ion dynamical broadening. From Eq. (A.8) we get  $\Gamma_i/\omega_{pi}\approx 13$ , so that the LEPT is quasistatic. Finally, from Eq. (A.7) we obtain  $F_{crit}\sim 400$  V/cm.

**Conflict of interest:** the authors declare no conflict of interest.

**Funding:** this work received no funding.

**Data availability:** all data is included in the paper.

## References

- 1. Griem HR. Principles of plasma spectroscopy. Cambridge: Cambridge University Press; 1997.
- 2. Fujimoto T. Plasma spectroscopy. Oxford, UK: Clarendon Press; 2004.
- 3. Oks E. Stark broadening of hydrogen and hydrogenlike spectral lines in plasmas: the physical insight. Oxford, UK: Alpha Science International; 2006.
- 4. Oks E. Diagnostics of laboratory and astrophysical plasmas using spectral lineshapes of one-, two-, and three-electron systems. Singapore: World Scientific; 2017.
- 5. Oks E. Advances in x-ray spectroscopy of laser plasmas. Bristol, UK: IOP Publishing; 2020.
- 6. U. Rebhan, N.J. Wiegart, H.-J. Kunze: Phys. Lett. **85** A, 228 (1981)
- 7. M.P. Brizhinev, V.P. Gavrilenko, S.V. Egorov, B.G. Eremin, A.V. Kostrov, E.A. Oks, Yu.M. Shagiev: Sov. Phys. JETP **58**, 517 (1983)
- 8. I.N. Polushkin, M.Yu. Ryabikin, Yu.M. Shagiev, V.V. Yazenkov: Sov. Phys. JETP **62**, 953 (1985)
- 9. U. Rebhan: J. Phys. B **19**, 3487 (1986)
- 10. R.A. Akhmedzhanov, I.N. Polushkin, Yu.V. Rostovtsev, M.Yu. Ryabikin, Yu.M. Shagiev, V.V. Yazenkov: Sov. Phys. JETP **63**, 30 (1986)

- 11. V.N. Aleinikov, B.G. Eremin, G.L. Klimchitskaya, I.N. Polushkin, Yu.V. Rostovtsev, V.V. Yazenkov: Sov. Phys. JETP **67**, 908 (1988)
- 12. Oks E. Plasma spectroscopy: the influence of microwave and laser fields. New York: Springer; 1995.
- 13. Oks E, Dalimier E, Faenov AY, Angelo P, Pikuz SA, Tubman E, et al. Using x-ray spectroscopy of relativistic laser plasma interaction to reveal parametric decay instabilities: a modeling tool for astrophysics. Optics Express 2017;25:1958-72.
- 14. Oks E, Dalimier E, Faenov AYa, Angelo P, Pikuz SA, Pikuz TA, et al. In-depth study of intra-Stark spectroscopy in the x-ray range in relativistic laser-plasma interactions. J Phys B: At Mol Opt Phys 2017;50:245006.
- 15. Oks E, Dalimier E, Angelo P, Pikuz T. Review of recent analytical advances in the spectroscopy of hydrogenic lines in plasmas. Open Physics **22** (2024) 20240002.
- 16. Lisitsa VS. Stark broadening of hydrogen lines in plasmas. Sov Phys Usp 1977;20:603-30.
- 17. Sholin GV, Oks E. Theory of optical polarization measurements of turbulence spectrum in plasmas. Sov Phys Doklady 1973;18:254-7.
- 18. Oks E, Sholin GV. On Stark profiles of hydrogen lines in a plasma with low-frequency turbulence. Sov Phys Tech Phys 1976;2<u>1</u>:144-51.
- 19. Strekalov ML, Burshtein AI. Collapse of shock-broadened multiplets. Soviet Phys JETP 72;343:53-58.
- 20. Idehara T, Sabchevski SP, Glyavin M, Mitsudo S. The gyrotrons as promising radiation sources for THz sensing and imaging. Appl Sci 2020;10:980.